Supplementary Information (SI) for Journal of Materials Chemistry C.

Supporting Information

Ionic Gating of a Meta-Connected Molecular Junction Achieves a 10^5 ON/OFF Ratio

Faizah Almutairi,[a†] Asma Alajmi,[ab†], Colin Lambert,[a] and Ali Ismael[ac*]

[a.] Physics Department, Lancaster University, Lancaster, LA1 4YB, UK.
[b.] Department of Physics, College of Science and Humanities in Al-Kharj, Prince Sattam Bin Abdulaziz University, Al-Kharj 11942, Saudi Arabia.
[c.] Department of Physics, College of Education for Pure Science, Tikrit University, Tikrit, Iraq.

† These authors contributed equally to this work
* k.ismael@lancaster.ac.uk

Contents

1. Theoretical details

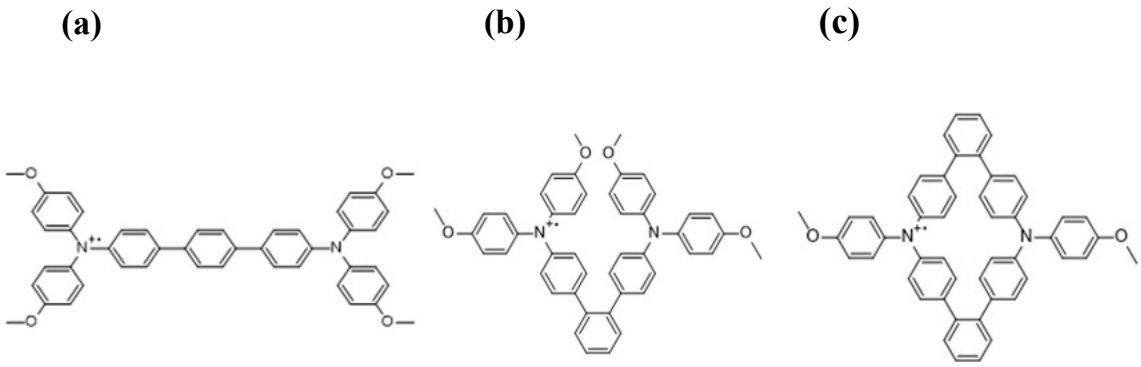

Figure S 1: Chemical structures of the studied molecules: (a) *para*-connected, (b) *ortho*-connected, and (c) *doubly bridged ortho*-connected configurations.

Figure S1 illustrates the chemical structures of the molecular systems investigated in this study, highlighting the different connectivity motifs used to probe charge-transport behavior. The *para-connected* configuration (Figure S1a) provides a linear and fully conjugated π-system, which is expected to facilitate efficient electron delocalization between the anchoring groups. In contrast, the *ortho-connected* structure (Figure S1b) introduces a more compact and angular geometry that disrupts π-conjugation, potentially reducing electronic coupling across the molecule. The *doubly bridged ortho-connected* architecture (Figure S1c) incorporates *two π-bridged* pathways, partially restoring conjugation relative to the single-*ortho* case while maintaining an overall non-linear topology. Together, these structures offer a systematic platform for assessing how molecular connectivity and conjugation pathways influence quantum interference and charge transport in single-molecule junctions.

1.1 Optimised DFT structures of isolated molecules

Density functional theory DFT code[1, 2],was used to determine the optimum geometries of the isolated molecules 1-3, through relaxing the molecules until the entire forces on the atoms have the value of <0.01 eV / Å.[1] This is shown in Figure S2. A double-zeta plus polarisation orbital basis set, norm-conserving pseudopotentials, with an energy cut-off of 250 Rydbergs are determined upon the real space grid for usage. The generalized gradient approximation GGA was adopted for exchange correlation functional.[3, 4]

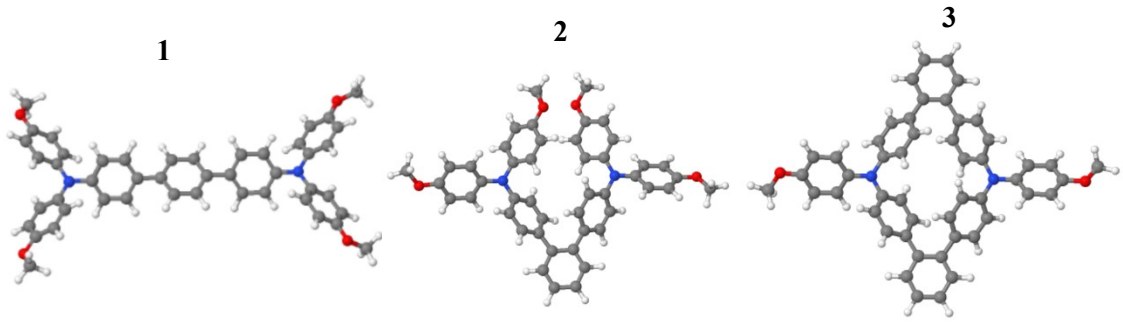

Figure S 2: Anthracene-based molecular junctions featuring O–Au anchoring groups with three distinct connectivities: (1) *para*-connected structure, (2) *ortho*-connected structure, and (3) *doubly π-bridged ortho*-connected structure.

Figure S2 shows three structures of anthracene-based molecules with different connectivities. These structures are fully relaxed, and are as follows, **1**: anthracene-based molecule with *para* connectivity and O–Au anchors, **2**: anthracene-based molecule with *ortho* connectivity and O–Au anchors, **3**: anthracene-based molecule with *doubly bridged (ortho)* connectivity and O–Au anchors.

These three structures correspond to the *para, ortho*, and *doubly-bridged ortho* connectivities used in this work. All geometries were fully relaxed using DFT before performing the transport calculations. The *para* structure provides a more extended conjugation pathway, the *ortho* structure introduces a twist in the backbone, and the *doubly-bridged ortho* partially restores conjugation relative to the *single-ortho* case.[5-7]

Because the molecules are treated in their radical-cation state, the total charge of the system becomes positive. To keep the system charge-neutral during the DFT calculations, a counter-ion (PF_6^-) was added. and then a PF_6^- ion was placed at different positions around the molecule and kept fixed during the transport calculations. Four positions were considered: near a carbon atom (Position 1), near the nitrogen atom of the amine centre (Position 2), and at the two ends of the oxygen anchoring group (Positions 3 and 4).[5, 8, 9]

1.2 Frontier orbitals of the molecules

The quantum state of molecules can be mathematically represented as a wave function. Wave functions provide considerable data relating to the position and motions of molecules. Moreover, they can be used to establish the probability density of an electron's position being found. [10, 11]

This section explains the frontier orbitals of the molecules being studied which are highest occupied molecular orbitals (HOMO), lowest unoccupied orbitals (LUMO), (HOMO-1), and (LUMO+1) as well as their energies.

1.2.1 *Para*-connected structure

$E_F = -2.14\ eV$

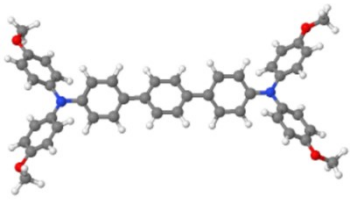

$HOMO = -3.47\ eV$

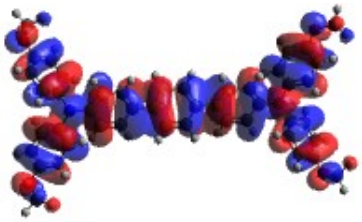

$LUMO = -1.18\ eV$

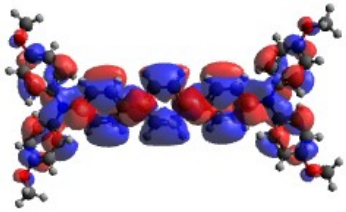

$HOMO - 1 = -3.62\ eV$

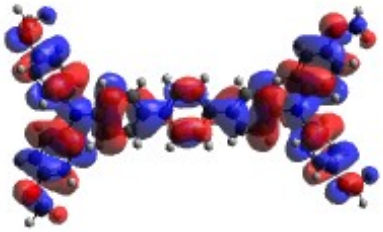

$LUMO + 1 = -0.82\ eV$

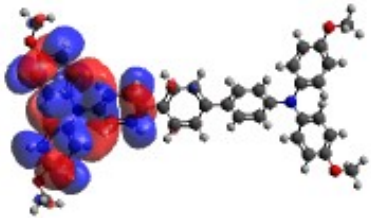

1.2.2. *Ortho*-connected structure

$E_F = -1.92\ eV$

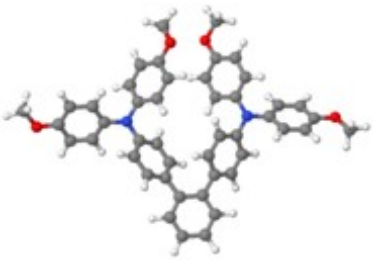

$HOMO = -3.42\ eV$

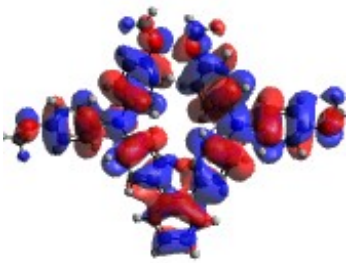

$LUMO = -1.13\ eV$

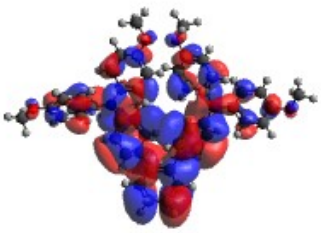

$HOMO - 1 = -3.58\ eV$

$LUMO + 1 = -0.88\ eV$

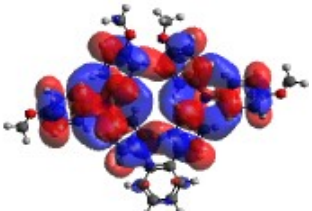

1.2.3. *Doubly π-bridged ortho*-connected structure

$E_F = -2.08\ eV$

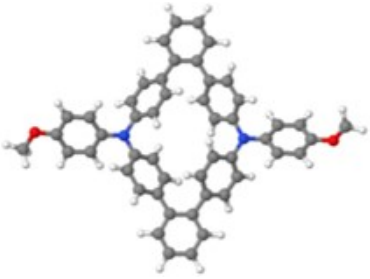

$HOMO = -3.52\ eV$

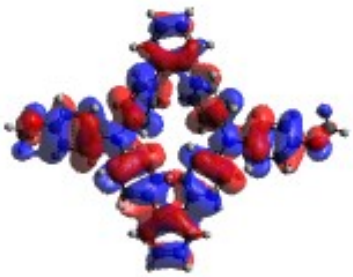

$LUMO = -1.42\ eV$

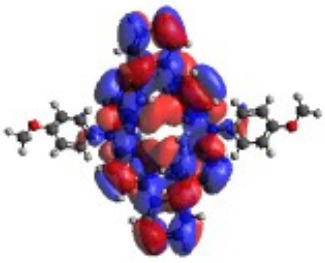

$HOMO - 1 = -3.78\ eV$

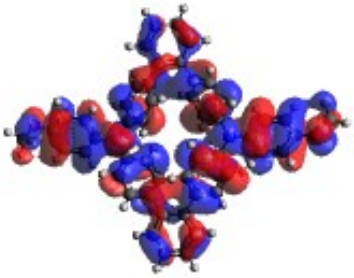

$LUMO + 1 = -1.06\ eV$

Figure S 5: Frontier molecular orbitals of the *doubly π-bridged ortho*-connected molecule. **Top**

2. Binding energy

This section explains the method that combines both DFT and the counterpoise. Counterpoise's role is to remove the basis set superposition errors during the calculation of the optimum binding distance of two objects[12]. The ideal distance separating the electrode from a molecule's specific atom can be established by calculating the binding energy. Initially, junctions between the lead and atoms are made using MATLAB and then the binding energy is calculated using SIESTA [13, 14].

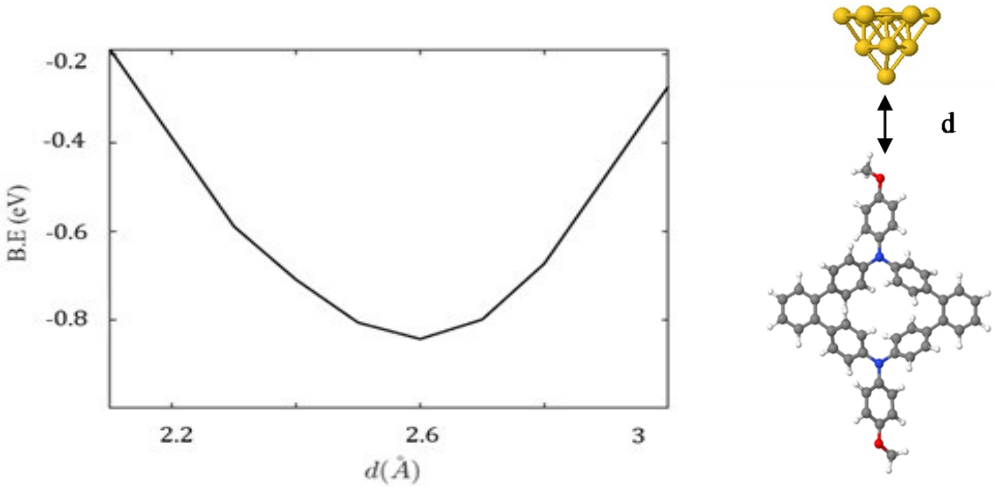

Figure S 6: Anthracene-based radical molecule in *ortho* configuration anchored via oxygen interaction with a gold electrode. **Right panel:** shows the fully optimised geometry. **Left panel**: presents the binding energy as a function of the Au–O distance The minimum binding energy is approximately at a distance of .

3. Transmission coefficient $T(E)$

The likelihood that an electron passes between the two electrodes via a molecule is referred to as the transmission coefficient[15, 16].

This section discusses the transmission function of benzothiadiazole-based molecules with different connectivities: *para, ortho, and ortho (doubly bridged)*.

3.1 *Para*-connected molecule

Figure S7 shows a *para*-connected molecule. The transmission curve indicates constructive quantum interference, giving relatively higher conductance compared to the other connectivities. The Fermi level is located close to the HOMO resonance, so the slope of $T(E)$ around E_F is small, resulting in a moderate positive Seebeck coefficient. This behaviour is typical for *para* connectivity, where electron pathways reinforce each other.

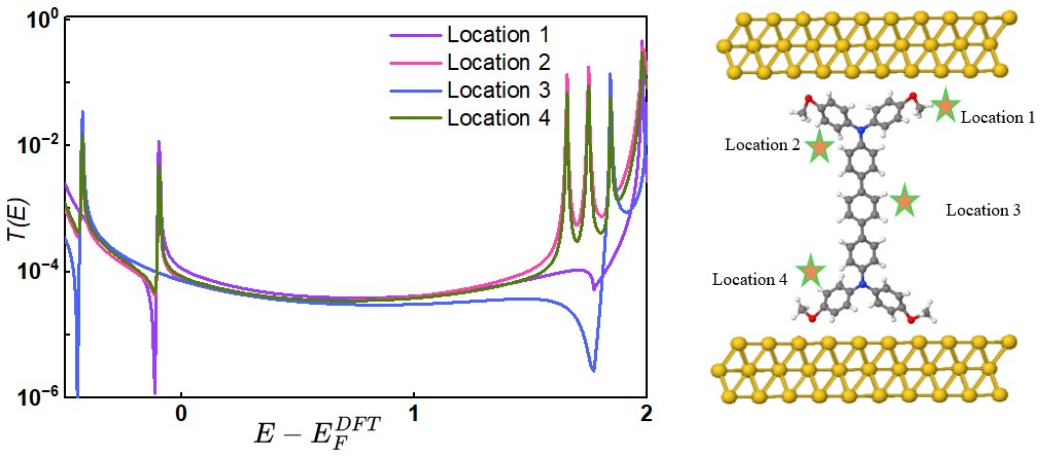

Figure S 7: **Right panel:** Schematic illustration of the *para-connected* junction showing the four possible locations of the counter-ion. **Left panel:** Zero-bias transmission coefficient of the *para-connected* molecule plotted as a function of electron energy . The star symbols indicate the presence of the ion. PF_6^-

3.2 *Ortho* -connected molecule

Figure S8 shows an *ortho-connected* molecule. In this case, the transmission is strongly affected by the *single ortho* connection, which shifts the spectral features slightly away from the Fermi level. As a result, $T(E)$ is reduced, but the slope around the Fermi energy becomes sharper, producing a larger positive Seebeck coefficient. This demonstrates how the *ortho* structure enhances thermoelectric response while lowering conductance.

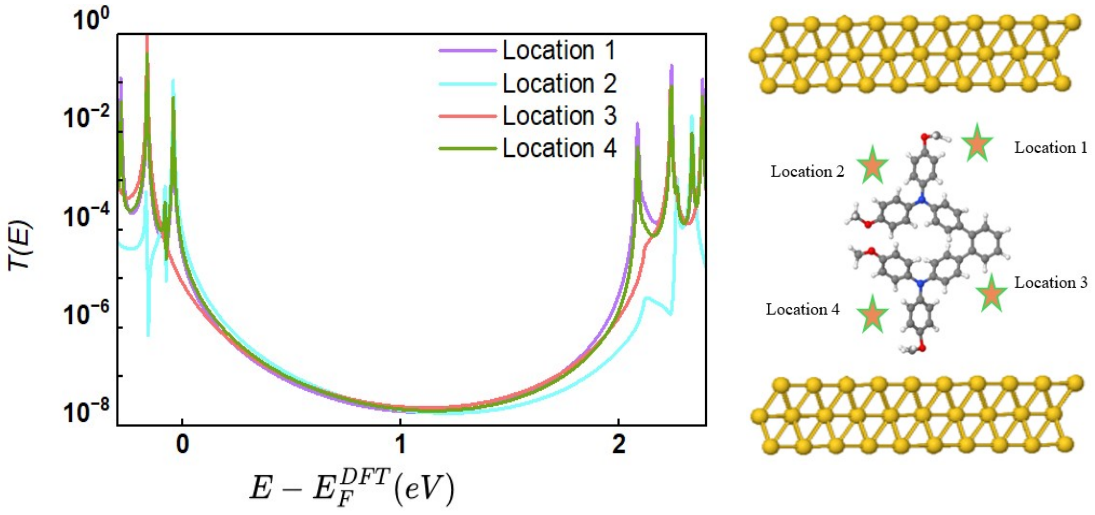

Figure S 8: **Right panel:** Schematic illustration of the *ortho-connected* junction showing the four possible locations of the counter-ion. **Left panel:** Zero-bias transmission coefficient of the *ortho-connected* molecule plotted as a function of electron energy . The star symbols indicate the presence of the ion. PF_6^-

3.3 *Doubly bridged ortho* -connected molecule

Figure S9 shows a *doubly bridged (ortho)-connected* molecule. In this case, the transmission is strongly affected by the presence of the two bridges, which shift spectral features closer to the Fermi level. As a result, $T(E)$ is suppressed but the slope around energy E. becomes very steep, producing a large positive Seebeck coefficient. This demonstrates how the *doubly bridged* structure enhances thermoelectric response while lowering conductance.

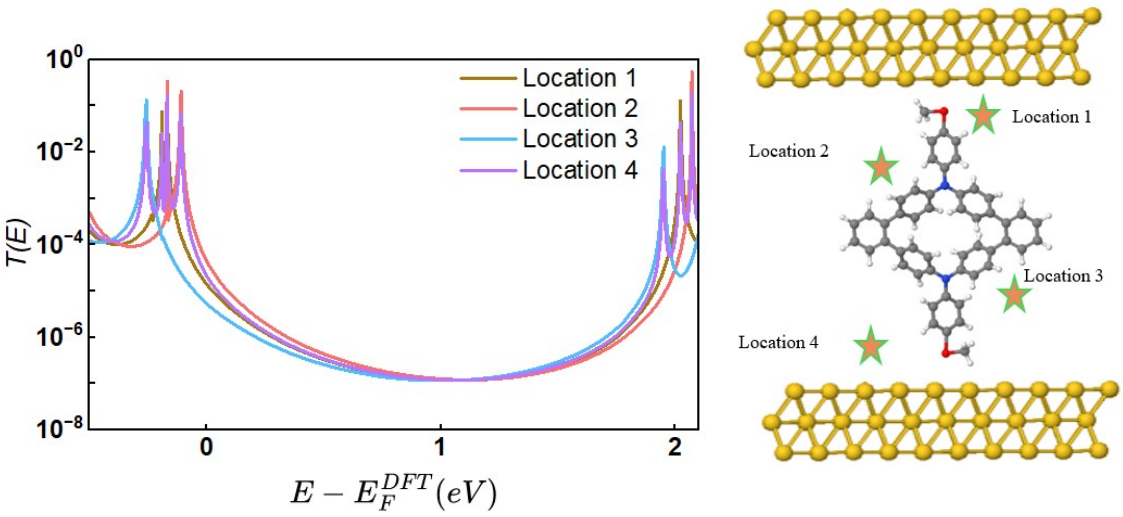

Figure S 9: **Right panel:** Schematic illustration of the *ortho*-connected junction showing the four possible locations of the counter-ion. **Left panel:** Zero-bias transmission coefficient of the *ortho*-connected molecule plotted as a function of electron energy . The star symbols indicate the presence of the ion. PF_6^-

4. Seebeck coefficient *S*

The Seebeck coefficients S are to be determined after the calculation is made upon the electronic transmission coefficient for the 3 junctions. Therefore, the introduction of the non-normalised probability distribution $P(E)$ defined by as defined below is justified. [16, 17]

$$P(E) = -T(E)\frac{df(E)}{dE} \quad \text{(S1)}$$

where $f(E)$ denotes the Fermi function and $T(E)$ denotes the transmission coefficients where Li are defined as:

$$L_i = \int dE\, P(E)(E - E_F)^i \quad \text{(S2)}$$

where, E_F is the Fermi energy. The Seebeck coefficient, S is then given by

$$S(T) = -\frac{L_1}{|e|TL_0} \quad \text{(S3)}$$

where, e is the electronic charge.

4.1 *Para*-connected molecule

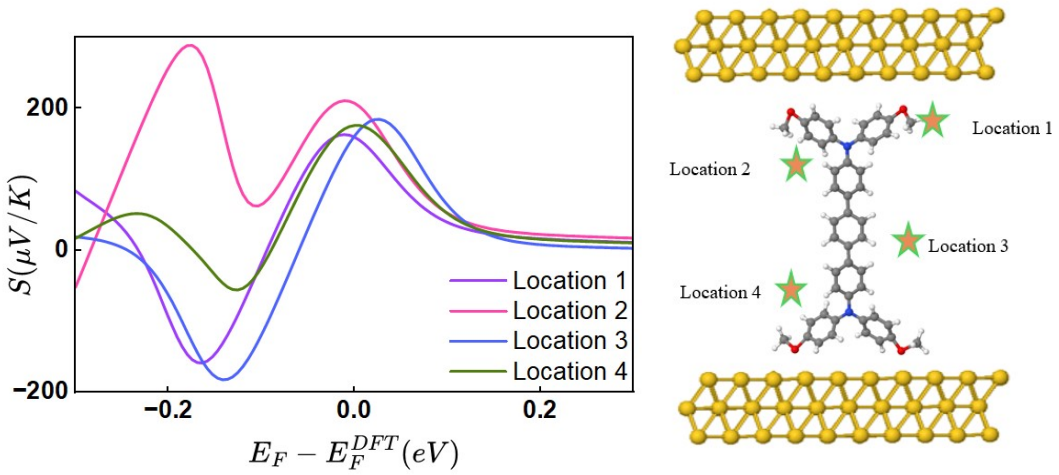

Figure S 10: **Right panel:** Schematic illustration of the *para-connected* junction showing the four possible locations of the counter-ion. **Left panel:** Seebeck coefficient of the *para-connected* molecule plotted as a function of electron energy . The star symbols indicate the presence of the ion. PF_6^-

In Figure S10 the *para-connected* molecule shows a moderate positive Seebeck coefficient at the DFT-predicted Fermi energy $E - E_F^{DFT} = 0\ eV$. This is consistent with HOMO-dominated transport, where the slope of the transmission function near the Fermi level is small.

4.2 *Ortho*-connected molecule

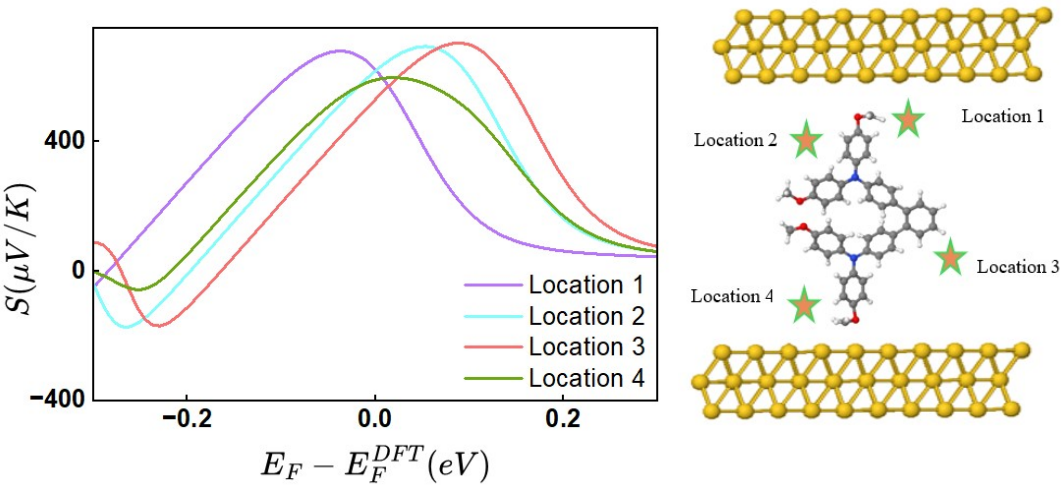

Figure S 11**: Right panel:** Schematic illustration of the *ortho-connected* junction showing the four possible locations of the counter-ion. **Left panel:** Seebeck coefficient of the *ortho-connected* molecule plotted as a function of electron energy . The star symbols indicate the presence of the ion. PF_6^-

4.3 *Double ortho*-connected molecule

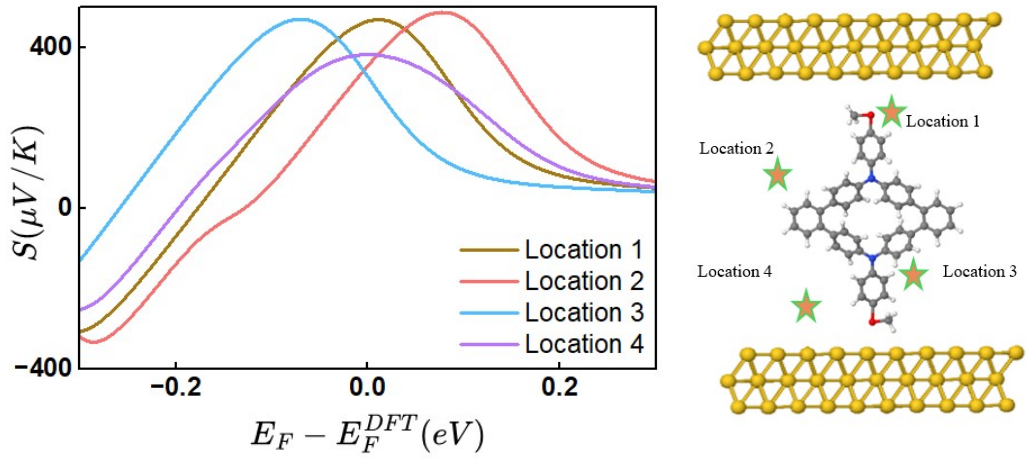

Figure S 12: **Right panel:** Schematic illustration of the *doubly bridged (ortho)-connected* junction showing the four possible locations of the counter-ion. **Left panel:** Seebeck coefficient of the *doubly bridged (ortho)-connected* molecule plotted as a function of electron energy . The star symbols indicate the presence of the ion.

5. New suggested *meta*-connected molecule

5.1 Introduction

After analysing the *para*, *ortho*, and *doubly bridged ortho* molecules, we extended our study to include a *meta-connected* junction. *Meta* connectivity is typically associated with lower conductance due to destructive quantum interference[8, 18], making it an interesting case to compare within the same radical-cation framework.

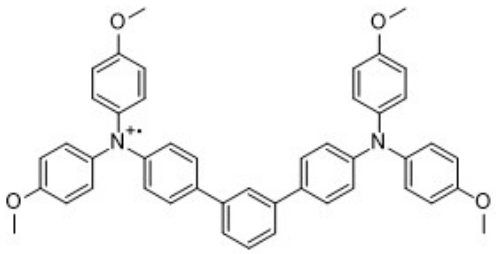

Figure S 13 : Chemical structure of *the meta-connected* configuration.

5.2 Optimised DFT *meta*-connected structure

The DFT code SIESTA can be used to relax isolated molecules so as to optimise their shapes[1, 2]. This relaxation procedure continues until the magnitude of the forces to which the atoms are subjected decline to less than $0.01\ eV/\text{Å}$ [1].

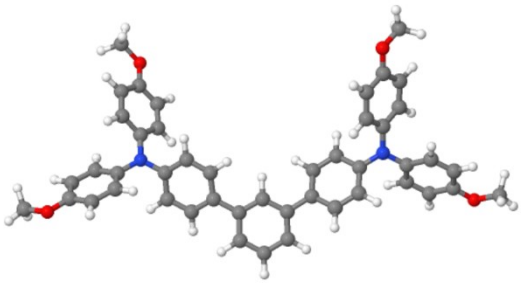

Figure S 14: Schematic structure of the *meta*-connected anthracene-based molecular junction with oxygen–gold (O–Au) anchoring groups.

5.3. Frontier orbitals of the *meta* connected molecule

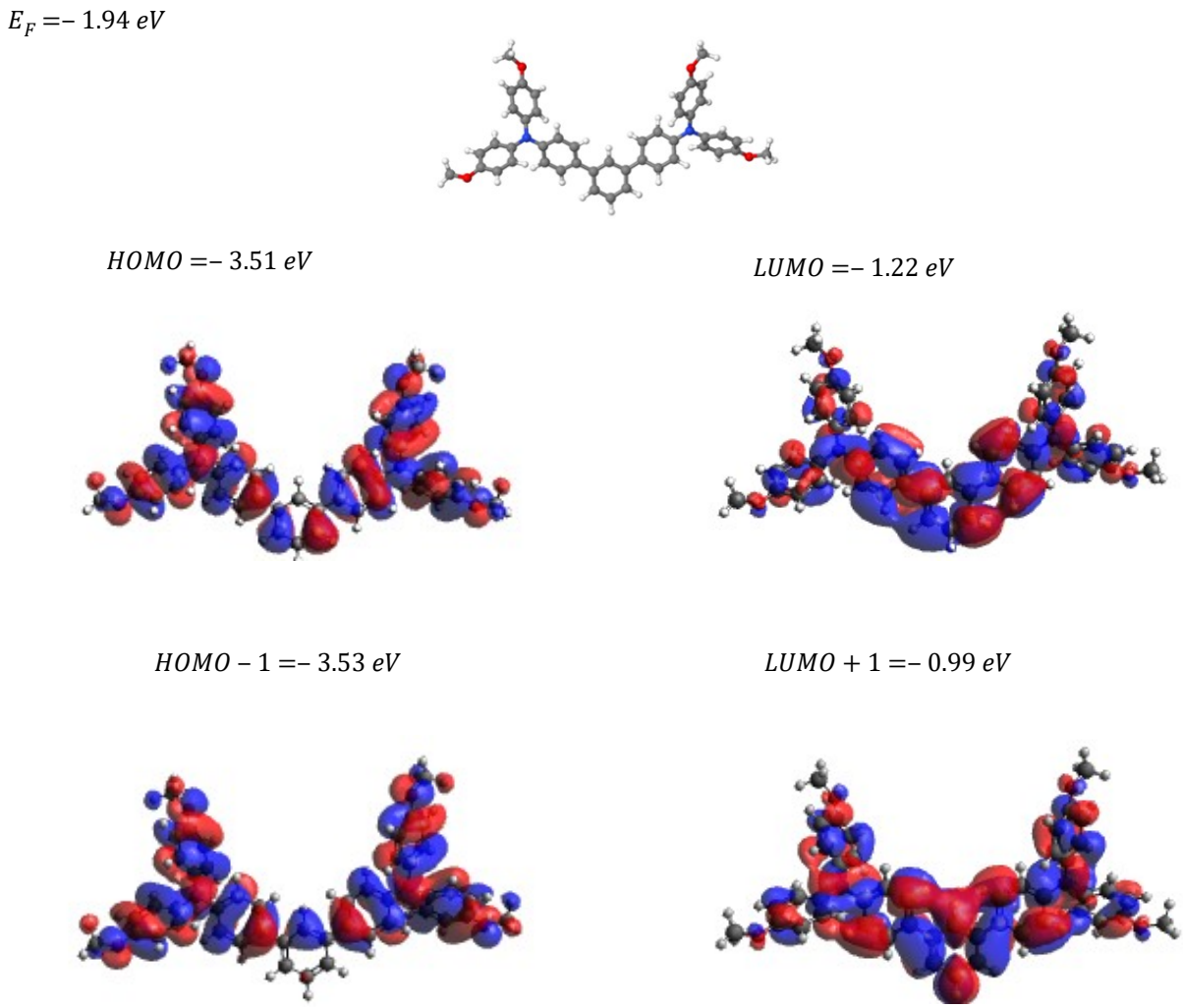

Figure S 15: Frontier molecular orbitals of the *meta*-connected molecule. **Top panel:** fully optimised geometry. **Bottom panel:** HOMO–1, HOMO, LUMO, and LUMO+1 orbitals with their energies relative to the Fermi level .

5.4 Transmission coefficient $T(E)$ of the *meta*-connected junction

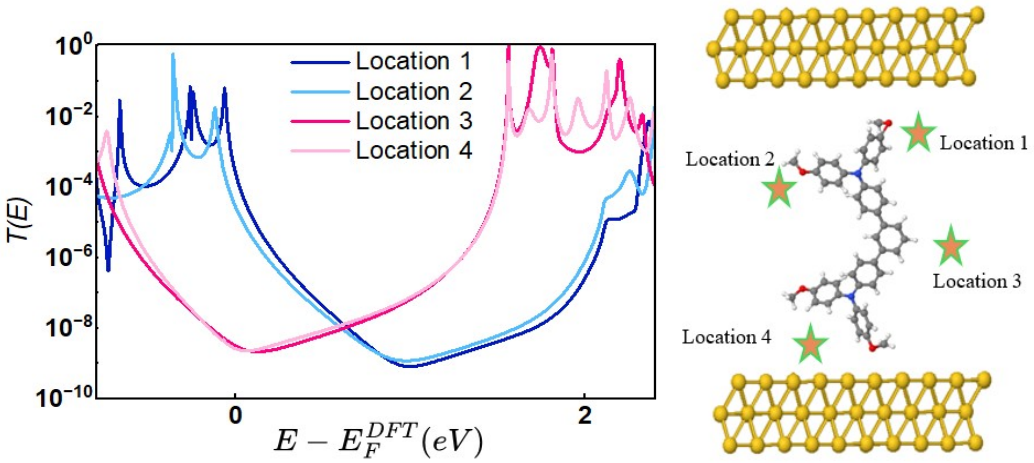

Figure S 16: **Right panel:** Schematic illustration of the *meta*-connected junction showing the four possible locations of the counter-ion. **Left panel:** Zero-bias transmission coefficient of the *meta*-connected molecule plotted as a function of electron energy . The star symbols indicate the presence of the ion. PF_6^-

5.5 Seebeck coefficient $S(E)$ of the *meta*-connected junction

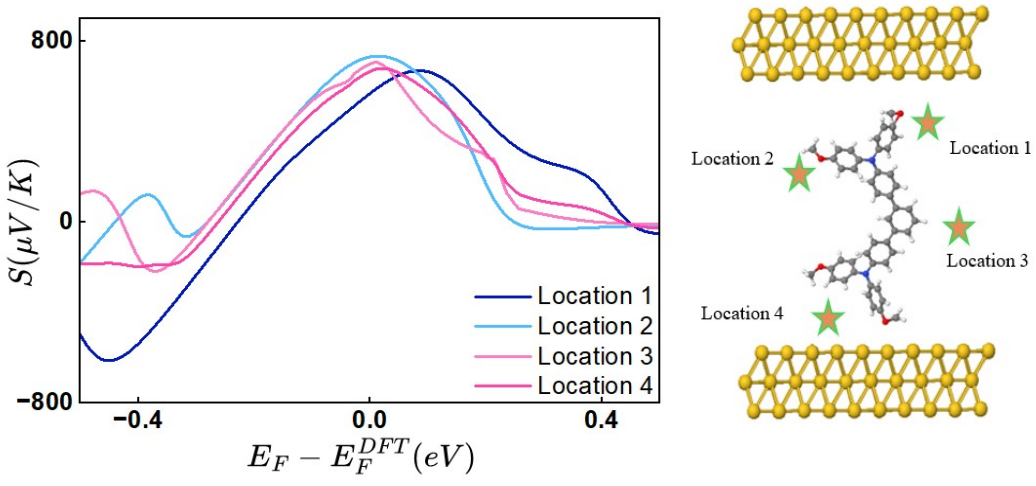

Figure S 17: **Right panel:** Schematic illustration of the *meta-connected* junction showing the four possible locations of the counter-ion. **Left panel:** Seebeck coefficient of the *meta-connected* molecule plotted as a function of electron energy . The star symbols indicate the presence of the

5.6 On-off ratio of the *meta* connected molecule

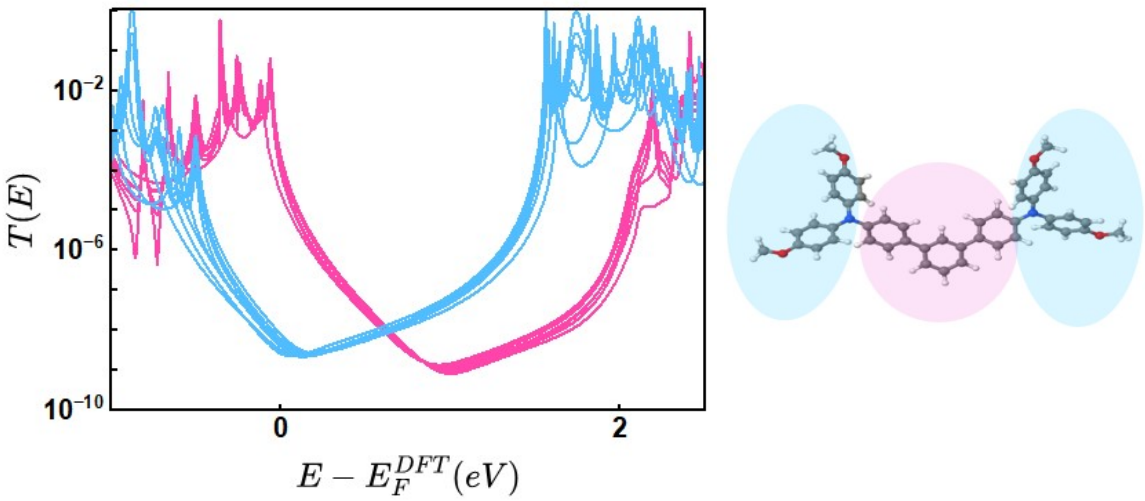

Figure S 18: **Left panel:** Transmission coefficient of the *meta-connected* molecule for different counter-ion positions**. Right panel:** Schematic illustration showing the four representative ion locations relative to the molecule. Counter-ions positioned near the anchoring groups suppress the transmission (OFF), whereas ions located near the molecular centre enhance it (ON), resulting in an ON/OFF ratio of approximately 10^5.

To investigate the ON/OFF behaviour, the counter-ion was moved systematically around the molecular backbone, and the transmission was recalculated at each position. As expected for

systems where local charge plays a decisive role, positions where the counter-ion sits near the anchoring groups reduce the effective coupling to the electrodes. In this configuration, the central conducting pathway remains largely unaffected while the end-group perturbation suppresses transmission, giving rise to the OFF state.

When the counter-ion moves towards the centre of the molecule, it alters the local charge distribution and reshapes the molecular orbitals in a way that enhances electronic communication across the junction. This leads to a clear increase in transmission, corresponding to the ON state.

This behaviour is fully consistent with what is known about charge-regulated quantum interference[19-22]: even small variations in the charge around a key atom can shift the balance between a destructive-interference pathway and a more efficient, high-conductance pathway. Such charge-controlled switching has been demonstrated in *meta-connected* heteroaromatic systems, where modifying the electron density on a single bridging atom changes the conductance by more than an order of magnitude.

In our *meta-connected* structure, a similar mechanism operates through counter-ion repositioning.

For the *meta system*, the transmission difference between the OFF and ON positions spans roughly two orders of magnitude, giving an ON/OFF ratio of ~10^5. By contrast, the *para system* remains highly conductive and only shows minor variations upon counter-ion displacement.

These results confirm that simple counter-ion movement is sufficient to switch the meta junction between ON and OFF states, whereas the *para junction* stays stable and strongly conductive.

6. Spin-polarized calculations

Spin-polarized calculations were performed to ensure a reliable description of the electronic structure of the molecular junctions studied. Ionic gating may modify the electronic structure and can give rise to possible open-shell configurations. Therefore,

treating spin explicitly allows such situations to be properly described and ensures a consistent evaluation of the electronic and transport properties. [8]

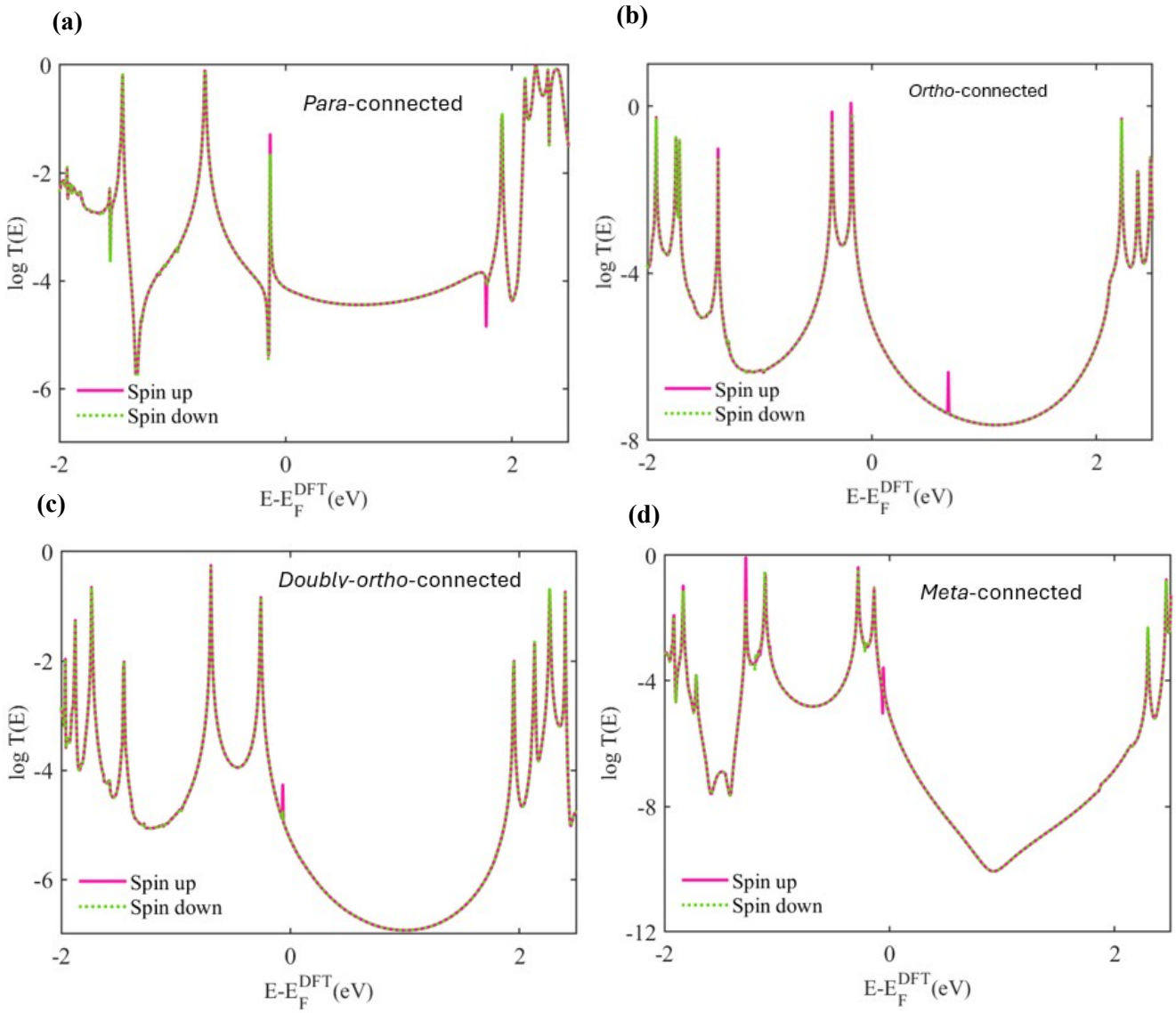

Figure S 19: Spin-polarized electron transmission spectra, as a function of energy relative to the DFT Fermi level ( ) for (a) *para*-connected, (b) *ortho*-connected, (c) *doubly-ortho*-connected, and (d) *meta*-connected molecular junctions. Spin-up and spin-down transmission channels are shown by solid magenta and dashed green lines, respectively. The near-perfect overlap of the two spin channels indicates negligible spin polarization in the transport for all connectivities considered.

$E - E_F^{DFT}$

7. Charge transfer analyses

Net atomic charge is a well-established concept that is widely employed across the chemical sciences.[23] Net atomic charge also plays an important role in molecular-scale systems, where charge redistribution influences electronic structure and transport properties.[8]

In this work, charge transfer is analysed for the *meta*-connected molecule using population analysis methods implemented in the SIESTA code, including Mulliken, Hirshfeld, and Voronoi charge analyses. The electronic behaviour of the *meta*-connected molecule is investigated in order to understand how charge transfer varies with counter-ion positioning.

Table 1. Charge analysis of the system with the PF_6^- counter-ion located at the molecular center and near the anchor group.

Method	**Position**	**Net charge (Molecule)**	**Net charge (Counter-ion)**	**Counter-ion**
Mulliken	Centre	+0.270	−0.260	Acceptor
Hirshfeld		+0.200	−0.201	
Voronoi		+0.182	−0.180	
Mulliken	Near anchor group	+0.508	−0.500	Acceptor
Hirshfeld		+0.505	−0.503	
Voronoi		+0.505	−0.507	

8. References

1. Soler, J.M., E. Artacho, J.D. Gale, A. García, J. Junquera, P. Ordejón, and D. Sánchez-Portal, *The SIESTA method for ab initio order-Nmaterials simulation.* Journal of physics: Condensed matter, 2002. **14**(11): p. 2745.
2. Artacho, E., E. Anglada, O. Diéguez, J.D. Gale, A. García, J. Junquera, R.M. Martin, P. Ordejón, J.M. Pruneda, and D. Sánchez-Portal, *The SIESTA method; developments and applicability.* Journal of Physics: Condensed Matter, 2008. **20**(6): p. 064208.
3. Herrer, I.L., A.K. Ismael, D.C. Milan, A. Vezzoli, S. Martín, A. González-Orive, I. Grace, C. Lambert, J.L. Serrano, and R.J. Nichols, *Unconventional single-molecule conductance behavior for a new heterocyclic anchoring group: pyrazolyl.* The journal of physical chemistry letters, 2018. **9**(18): p. 5364-5372.
4. Peng, H. and J.P. Perdew, *Rehabilitation of the Perdew-Burke-Ernzerhof generalized gradient approximation for layered materials.* Physical Review B, 2017. **95**(8): p. 081105.
5. Yoshida, K., F. Takasaki, M. Uebe, S. Seki, and A. Ito, *Impact of Double-π-Bridge on Bis (Triarylamine)-Based Organic Mixed-Valence System: A Case Study of Diaza [1.1](4, 4") ortho-Terphenylophane Radical Cation.* Chemistry–A European Journal, 2025. **31**(6): p. e202403945.
6. Shiri, M., H. Zhang, and K. Wang, *No More Conductance Decay: Toward Efficient Long-Range Transport in Molecular Wires.* ACS Applied Electronic Materials, 2024. **6**(12): p. 8626-8639.
7. Prindle, C.R., W. Shi, L. Li, J. Dahl Jensen, B.W. Laursen, M.L. Steigerwald, C. Nuckolls, and L. Venkataraman, *Effective gating in single-molecule junctions through fano resonances.* Journal of the American Chemical Society, 2024. **146**(6): p. 3646-3650.
8. Lambert, C., *Basic concepts of quantum interference and electron transport in single-molecule electronics.* Chemical Society Reviews, 2015. **44**(4): p. 875-888.
9. Manrique, D.Z., C. Huang, M. Baghernejad, X. Zhao, O.A. Al-Owaedi, H. Sadeghi, V. Kaliginedi, W. Hong, M. Gulcur, and T. Wandlowski, *A quantum circuit rule for interference effects in single-molecule electrical junctions.* Nature communications, 2015. **6**(1): p. 6389.
10. Finch, C.M., S. Sirichantaropass, S.W. Bailey, I.M. Grace, V.M. Garcia-Suarez, and C.J. Lambert, *Conformation dependence of molecular conductance: chemistry versus geometry.* Journal of Physics: Condensed Matter, 2007. **20**(2): p. 022203.
11. Ismael, A.K. and C.J. Lambert, *Molecular-scale thermoelectricity: a worst-case scenario.* Nanoscale Horizons, 2020. **5**(7): p. 1073-1080.
12. Haynes, P., C.-K. Skylaris, A. Mostofi, and M. Payne, *Elimination of basis set superposition error in linear-scaling density-functional calculations with local orbitals optimised in situ.* Chemical physics letters, 2006. **422**(4-6): p. 345-349.
13. Alagona, G., C. Ghio, Z. Latajka, and J. Tomasi, *Basis set superposition errors and counterpoise corrections for some basis sets evaluated for a few X-. cntdot.. cntdot.. cntdot. M dimers.* Journal of Physical Chemistry, 1990. **94**(6): p. 2267-2273.
14. Daza, M.C., J. Dobado, J.M. Molina, P. Salvador, M. Duran, and J.L. Villaveces, *Basis set superposition error-counterpoise corrected potential energy surfaces. Application to hydrogen peroxide⋯ X (X= F−, Cl−, Br−, Li+, Na+) complexes.* The Journal of chemical physics, 1999. **110**(24): p. 11806-11813.

15. Al-Khaykanee, M.K., A.K. Ismael, I. Grace, and C.J. Lambert, *Oscillating Seebeck coefficients in π-stacked molecular junctions.* RSC advances, 2018. **8**(44): p. 24711-24715.
16. Alshammari, M., A.A. Al-Jobory, T. Alotaibi, C.J. Lambert, and A. Ismael, *Orientational control of molecular scale thermoelectricity.* Nanoscale Advances, 2022. **4**(21): p. 4635-4638.
17. Ismael, A.K., I. Grace, and C.J. Lambert, *Increasing the thermopower of crown-ether-bridged anthraquinones.* Nanoscale, 2015. **7**(41): p. 17338-17342.
18. Hybertsen, M.S., L. Venkataraman, J.E. Klare, A.C. Whalley, M.L. Steigerwald, and C. Nuckolls, *Amine-linked single-molecule circuits: systematic trends across molecular families.* Journal of physics: Condensed matter, 2008. **20**(37): p. 374115.
19. Evers, F., R. Korytár, S. Tewari, and J.M. Van Ruitenbeek, *Advances and challenges in single-molecule electron transport.* Reviews of Modern Physics, 2020. **92**(3): p. 035001.
20. Solomon, G.C., D.Q. Andrews, R.H. Goldsmith, T. Hansen, M.R. Wasielewski, R.P. Van Duyne, and M.A. Ratner, *Quantum interference in acyclic systems: Conductance of cross-conjugated molecules.* Journal of the American Chemical Society, 2008. **130**(51): p. 17301-17308.
21. Markussen, T., J. Schiötz, and K.S. Thygesen, *Electrochemical control of quantum interference in anthraquinone-based molecular switches.* The Journal of chemical physics, 2010. **132**(22).
22. Naghibi, S., A.K. Ismael, A. Vezzoli, M.K. Al-Khaykanee, X. Zheng, I.M. Grace, D. Bethell, S.J. Higgins, C.J. Lambert, and R.J. Nichols, *Synthetic control of quantum interference by regulating charge on a single atom in heteroaromatic molecular junctions.* The journal of physical chemistry letters, 2019. **10**(20): p. 6419-6424.
23. Shusterman, A.J. and L.M. Hoistad, *Teaching chemistry with electron density models. 2. Can atomic charges adequately explain electrostatic potential maps?* The Chemical Educator, 2000. **6**(1): p. 36-40.